doi:10.1016/j.jmb.2004.07.070 J. Mol. Biol. (2004) 342, 1085–1099

JMB

Available online at www.sciencedirect.com

SCIENCE DIRECT®

ELSEVIER

Transcription Factors IIF and IIS and Nucleoside Triphosphate Substrates as Dynamic Probes of the Human RNA Polymerase II Mechanism

Chunfen Zhang and Zachary F. Burton*

Department of Biochemistry and Molecular Biology Michigan State University E. Lansing, MI 48824-1319 USA

**Corresponding author*

The mechanism for elongation catalyzed by human RNA polymerase II (RNAP II) has been analyzed using millisecond phase transient state kinetics. Here, we apply a running start, two-bond, double-quench protocol. Quenching the reaction with EDTA indicates NTP loading into the active site followed by rapid isomerization. HCl quenching defines the time of phosphodiester bond formation. Model-independent and global kinetic analyses were applied to simulate the RNAP II mechanism for forward elongation through the synthesis of two specific phosphodiester bonds, modeling rate data collected over a wide range of nucleoside triphosphate concentrations. We report adequate two-bond kinetic simulations for the reaction in the presence of TFIIF alone and in the presence of TFIIF+TFIIS, providing detailed insight into the RNAP II mechanism and into processive RNA synthesis. RNAP II extends an RNA chain through a substrate induced-fit mechanism, termed NTP-driven translocation. After rapid isomerization, chemistry is delayed. At a stall point induced by withholding the next templated NTP, RNAP II fractionates into at least two active and one paused conformation, revealed as different forward rates of elongation. In the presence of TFIIF alone or in the presence of TFIIF+TFIIS, rapid rates are very similar; although, with TFIIF alone the complex is more highly poised for forward synthesis. Based on steady-state analysis, TFIIF was thought to suppress transcriptional pausing, but this view is misleading. TFIIF supports elongation and suppresses pausing by stabilizing the post-translocated elongation complex. When TFIIS is present, RNA cleavage and transcriptional restart pathways are supported, but TFIIS has a role in suppression of transient pausing, which is the most important contribution of TFIIS to elongation from a stall position.

Keywords: NTP-driven translocation; transient state kinetics; RNA polymerase II; transcription factor IIF; transcription factor IIS

Introduction

Transient state kinetic analysis allows an enzyme reaction to be tracked in real time through individual catalytic events,[1,2] and correlating enzyme functional dynamics with structural information allows inference of the most reasonable reaction mechanism. Using rapid quench-flow technology, our laboratory has begun to analyze the formation of multiple specific phosphodiester bonds during elongation by human RNA polymerase II (RNAP II).[3–5] Rapid chemical quench-flow techniques allow the RNAP II reaction to be tracked with millisecond precision, allowing characterization of all but the very fastest rates of bond formation. These studies provide significant insight into active site isomerization, phosphodiester bond formation, translocation, processive elongation, transcriptional stalling, pausing, RNA cleavage and restart from a shortened RNA 3′ end.

In recent studies of poliovirus RNA-dependent RNA polymerase, Cameron and colleagues[6,7] demonstrated that EDTA and HCl quenched

Abbreviations used: TFIIF, transcription factor IIF; TFIIS, transcription factor IIS; NTPs, nucleoside triphosphates; RNAP, RNA polymerase; DNAP, DNA polymerase; EC, elongation complex.

E-mail address of the corresponding author: burton@msu.edu

elongation at different reaction stages, when the reaction was run in the presence of Mn^{2+} as the divalent cation. This result indicated that the elongation complex (EC) isomerized to sequester two active site Mn^{2+} atoms from EDTA chelation and that, after EDTA addition, the isomerized EC continued on the forward pathway to complete bond formation. HCl was expected to quench the reaction instantly, demonstrating the time of chemistry. We wished to determine, therefore, whether the human RNAP II elongation mechanism could similarly be divided into stages, according to the time of Mg^{2+} sequestration (isomerization) and the time of phosphodiester bond synthesis (chemistry). Applying this double-quench approach, we obtain a more detailed view of the human RNAP II mechanism.

Here, we compare elongation in the presence of transcription factor IIF (TFIIF) and in the presence of TFIIF + TFIIS. TFIIF stimulates elongation by RNAP II five- to tenfold in steady-state analysis,[8–13] and TFIIF is also required during the initiation phase of the transcription cycle. TFIIS rescues stalled RNAP II ECs. In the presence of substrate nucleoside triphosphates (NTPs), TFIIS helps restart elongation by inducing cleavage of the nascent RNA chain, primarily in dinucleotide increments. TFIIS can also stimulate cleavage of larger RNA segments from previously backtracked and arrested ECs.[14–17] Recent work from our laboratory, however, indicates that TFIIS has an activity that does not depend on RNA cleavage, because TFIIS can also suppress transient transcriptional pausing.[3] Functions of TFIIS were recently illuminated by an X-ray crystal structure of yeast RNAP II bound to TFIIS.[18]

Figure 1 demonstrates our model for NTP loading and NTP-driven translocation of template DNA and the RNA–DNA hybrid during transcription by RNAP II. In the yeast RNAP II EC,[19,20] template DNA bends at about 90 degrees over the bridge α-helix. Incoming duplex DNA flows into the structure through the RNAP II "jaws". The RNA–DNA hybrid diverges from incoming DNA, because DNA bends over the bridge helix and because of the packing of the RNA–DNA hybrid in the structure. The eight to nine base-pair hybrid is constrained by the "clamp" and "wall" domains and pressed against the bridge α-helix at the site of chemistry. Like DNA polymerases (DNAPs), RNAP II utilizes a two-Mg^{2+} catalytic mechanism (metals A and B).[19–25] Three unpaired DNA bases ($n+1$, $n+2$, $n+3$; n = RNA length) are observed projecting into the main RNAP II channel, indicating that NTPs can pair with cognate DNA bases in the main channel.[5,19,26] The secondary pore of RNAP II provides another solvent-accessible route to the active site and may provide a second channel for NTP loading.[19,21,24,27] In the pre-translocated EC, however, approach of the RNA–DNA hybrid toward the bridge α-helix is expected to block NTP access through the secondary pore. Furthermore, prior to translocation, the $n+1$ cognate DNA base projects into the main enzyme channel not the secondary pore.[19]

Kinetic studies from our laboratory indicated that, during processive RNA synthesis, NTPs pair with their cognate DNA base prior to translocation.[5] This result suggests that, under physiological elongation conditions, the main enzyme channel provides the primary route of NTP entry into the RNAP II active site. After translocation, the $n+1$ DNA template base projects into the secondary pore, making the pore the likely route of NTP loading into the post-translocated EC.[20] We suggest that both the main enzyme channel and the secondary pore must be routes for NTP loading, depending on the translocation state of the EC.

NTP-driven translocation is a special case of substrate induced-fit, in which the incoming NTP substrate pairs with its cognate DNA base prior to DNA duplex and RNA–DNA hybrid translocation and movement of the NTP-dNMP base-pair into the active site for chemistry. We proposed that NTP-driven translocation is a primary determinant of transcriptional fidelity, because accurate base-pairing is a prerequisite for translocation, and translocation is required for chemistry.[5] Incorporation of an incorrectly specified base, therefore, is largely prevented, because mispaired NTPs do not drive translocation. Based on the X-ray structure of the yeast RNAP II EC, we proposed a model for NTP-induced translocation, in which NTPs load through the main RNAP II channel, in the same direction of flow as incoming duplex DNA. After pairing of incoming NTPs with single-stranded DNA cognate bases that face the main channel, the $n+1$ NTP enters the active site, paired with its template DNA base, as translocation proceeds. After chemistry, pyrophosphate is released into the secondary pore. Here, we affirm and extend the NTP-driven translocation model. A similar model for NTP-stimulated translocation, termed the "allosteric" model, was recently suggested for elongation by *Escherichia coli* RNAP,[26,28] which is a multi-subunit homolog of human RNAP II.

Using the potent inhibitor α-amanitin as a probe of the RNAP II elongation mechanism, we have obtained strong support for a major tenet of the NTP-driven translocation mechanism.[29] NTP-driven translocation requires two conformations of the RNAP II EC on the active synthesis pathway, each capable of binding NTPs: (1) post-translocated; and (2) pre-translocated. These ECs are observed to have different responses to NTP substrates and might show different sensitivities to inhibitors. Kornberg's laboratory reported a structure of yeast RNAP II soaked with the mushroom toxin α-amanitin, which was located bound to the Rpb1 bridge α-helix,[30] thought to be essential in translocation mechanisms.[19,24] Indeed, we find that α-amanitin blocks the reaction phase we had previously identified as the translocation step. The EC that we identify as post-translocated is completely insensitive to α-amanitin inhibition for formation of a single phosphodiester bond but

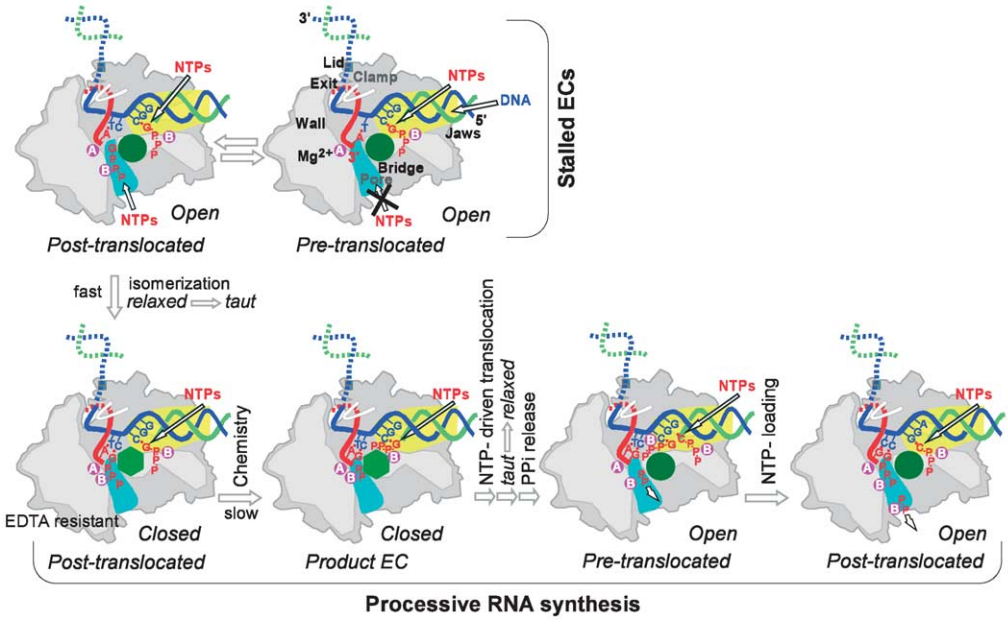

Figure 1. Routes of NTP loading into the RNAP II EC and the NTP-driven translocation model. When stalled by deprivation of the next substrate NTP, the RNAP II EC fractionates into pre-translocated and post-translocated conformations. The pre-translocated EC pairs the $n+1$ NTP (n=RNA length) to its cognate DNA base, which projects into the main enzyme channel (yellow shading). The post-translocated EC most likely loads the $n+1$ substrate NTP through the secondary pore (light blue shading) and the $n+2$ NTP through the main channel. During processive synthesis, NTPs load continuously through the main RNAP II channel, and NTPs are loaded into the active site by NTP-driven translocation. The DNA template strand is dark blue; the non-template strand is light green; the bridge α-helix is dark green (circle, open active site conformation; hexagon, closed active site conformation); the DNA duplex and RNA–DNA hybrid fill the enzyme main channel; PPi indicates pyrophosphate; Mg^{2+} A and B are indicated in magenta.

becomes highly sensitive to inhibition in the subsequent bond addition cycle, indicating that α-amanitin blocks translocation. The EC that we identify as pre-translocated is fully sensitive to α-amanitin inhibition. These results confirm that RNAP II has a minimum of two active conformations with distinct elongation kinetics and differential sensitivity to α-amanitin, affirming this key aspect of the NTP-driven translocation model.

In other work, we analyzed the pausing, RNA cleavage and restart pathways for human RNAP II.[3] The strategy was to stall RNAP II at a particular base position and determine how the enzyme fractionates between active and paused elongation modes. This analysis was done in the presence of TFIIF, TFIIS and hepatitis δ antigen, a viral elongation factor. From these studies a model was developed identifying five distinct ECs: (1) post-translocated; (2) pre-translocated; (3) paused (pre-translocated but not further backtracked); (4) backtracked (backtracked by one nucleotide from the pre-translocated state); and (5) cleaved (dinucleotide released, poised for restart). A similar analysis of human RNAP II elongation and pausing was presented by Palangat & Landick,[31] based on studies of the strong HIV-1 LTR pause site just downstream of *tar*. Their studies affirm many aspects of our model. In our laboratory, analysis of stalling revealed an interesting combinatorial effect of TFIIF and TFIIS in elongation, which we employ here. In the presence of both TFIIF and TFIIS, RNAP II elongation rates are as rapid as in the presence of TFIIF alone, but TFIIS suppresses transcriptional pausing, making forward elongation more efficient.[3] According to our model for the pausing, backtracking, RNA cleavage and restart pathways, we define transient transcriptional pausing as an early intermediate into backtracked, cleaved and arrested modes. This definition is supported by recent single molecule studies of transiently paused *E. coli* RNAP ECs.[32,33]. TFIIS appears to accelerate the rates into and out of this paused conformation of the RNAP II EC.[3] Enhancing the efficiency of elongation with TFIIS greatly improves the kinetic analysis of RNAP II elongation, in addition to providing insight into regulation of elongation by TFIIF and TFIIS. Comparison of the reaction mechanism in the presence of TFIIF alone and in the presence of both TFIIF and TFIIS refines our understanding of the mechanism for RNA synthesis and provides insight into translocation, NTP loading and allosteric effects of TFIIF and TFIIS in elongation control.

Results

TFIIS improves the efficiency, and TFIIF stimulates the rate of RNAP II elongation

In previous work, we indicated that TFIIF and TFIIS can cooperate to suppress transcriptional

pausing at a stall position.[3] In Figure 2, we support this observation by analyzing RNAP II elongation in the absence of elongation factors, in the presence of TFIIS, in the presence of TFIIF and in the presence of TFIIF+TFIIS. In Figure 2A, this comparison is done at 5 μM GTP, a limiting concentration of NTP substrate. In Figure 2B, the comparison is shown at 2500 μM GTP. The physiological GTP concentration for mammalian cells and tissues is reported as 470 μM,[34] but elongation rates continue to increase above physiological NTP levels. The running start, two-bond protocol[3–5,13] is described at the top of the Figure.

Elongation proceeds through the sequence 40-CAAAGG-45, starting at the C40 position (a 40-nucleotide RNA ending in a 3′-CMP). The EC is advanced to the A43 position by addition of ATP for 30–120 seconds, during which time ECs immobilized on beads are transferred into the sample port of the RQF-3 Rapid Chemical Quench-Flow instrument. ECs are then rapidly mixed with GTP, and the reaction quenched with EDTA after 0.002 to 0.5 s. The data are compared for the G44 synthesis rate, reported as G44 plus longer transcripts (G44+%) plotted as a function of the elongation time. In the presence of TFIIF alone or in the presence of both TFIIF and TFIIS, elongation rates are very similar, but, when both TFIIF and TFIIS are present, a larger proportion of ECs advance from the A43 stall point in 0.5 second (Figure 2B; >80% *versus* <60%). We attribute the >20% improvement in elongation efficiency in the presence of TFIIS to suppression of transcriptional pausing.[3] In our analysis, TFIIF appears to be the major stimulant of the elongation rate, and TFIIS appears to improve elongation efficiency, particularly in the presence of TFIIF. Comparing elongation in the absence of a stimulatory elongation factor with elongation in the presence of TFIIS alone, rates are similar. TFIIS stimulates the efficiency of RNAP II elongation at 2500 μM GTP (Figure 2B) but this effect is not noticeable at 5 μM GTP (Figure 2A). We conclude that TFIIF stimulates elongation rate. TFIIS suppresses transient transcriptional pausing, and this effect is most apparent in the presence of TFIIF.

TFIIF promotes a highly poised conformation of the RNAP II EC

We experienced difficulties obtaining a suitable kinetic data set using TFIIF as the sole stimulatory elongation factor.[5] The problem we encountered was that TFIIF appeared to support a highly poised EC that was capable either of scavenging trace GTP or of misincorporation of AMP for GMP, extending the chain from A43→G44 or *A44 (indicating misincorporation of AMP). Inappropriate NMP incorporation at the stall position was a particular problem for obtaining an interpretable kinetic data set, because adjusting the background for G44 (*A44) synthesis could not be done objectively. For the experiment shown in Figure 3, the running start assay was done in the presence of TFIIF or TFIIF+TFIIS through the 40-CAAAGG-45 sequence. In the presence of TFIIF alone, the C40 stall position is overrun by incorporation of AMP from trace ATP to synthesize A41 (lane 1), and the A43 stall position is overrun to synthesize G44 or *A44 (lanes 2–5). The problem of overrunning stall positions is alleviated by addition of TFIIS to the reaction (lanes 7–11). This result indicates that trace ATP and GTP are not likely to substantially contaminate the TFIIF preparation, because TFIIF is present in all reactions. Furthermore, scavenging of rare NTPs and/or misincorporation in the presence of TFIIF is a property of the EC in the presence of TFIIF alone but not of the EC in the presence of both TFIIF and TFIIS. We conclude that the RNAP II EC is very highly poised for RNA synthesis at the stall position in the presence of TFIIF alone but less highly poised in the presence of TFIIF and TFIIS. In other experiments, we determined that background incorporation of GMP at the A43 stall position could be minimized by collecting the TFIIF kinetic data set using a 10 μM rather than a 100 μM ATP pulse.

Regulation of RNAP II elongation by TFIIF and TFIIF+TFIIS

To more fully characterize the effects of

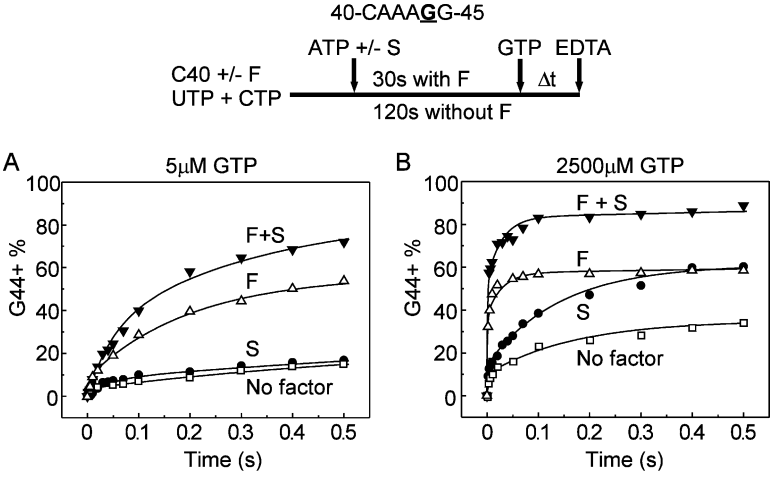

Figure 2. TFIIF stimulates elongation rate, and TFIIS improves elongation efficiency in the presence of TFIIF. Elongation rates for G44 synthesis are shown, at 5 μM (A) and 2500 μM GTP (B). G44+% indicates G44 plus all longer transcripts, expressed as % of total ECs. The reaction protocol is indicated at the top of the Figure. F indicates TFIIF; S indicates TFIIS.

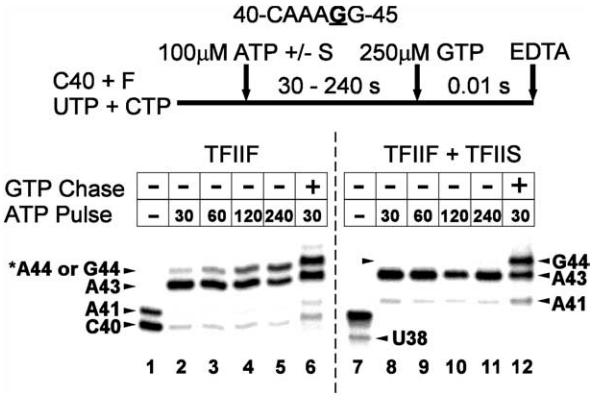

Figure 3. TFIIF supports a highly poised conformation of the EC that is not supported in the presence of both TFIIF and TFIIS. This conclusion is indicated by apparent scavenging of trace ATP and GTP by the stalled C40 and A43 ECs and/or misincorporation of AMP for GMP at A43. The protocol is shown at the top of the Figure. The 100 μM ATP pulse time was 0, 30, 60, 120 or 240 seconds, as indicated. The 250 μM GTP chase was for 0.01 second (lanes 6 and 12 only). F indicates TFIIF; S indicates TFIIS.

elongation factors on pausing, nascent RNA cleavage and forward synthesis, we analyzed RNAP II elongation rates at many different substrate GTP concentrations, in the presence of TFIIF alone and in the presence of both TFIIF and TFIIS. Typical elongation assay data are shown in Figure 4, using an EDTA quench protocol. We previously reported analysis of RNAP II elongation in the presence of TFIIF, but, in the course of the current studies, we learned that the previous analysis could be improved. All of the data shown here are newly acquired. For the reaction with TFIIF alone, we used a 10 μM ATP pulse to suppress background G44 and/or *A44 synthesis (Figure 3). In control experiments (not shown), we determined that lowering the ATP concentration did not noticeably affect elongation rates to G44 and G45 but successfully reduced background G44 synthesis. In the presence of both TFIIF and TFIIS, the EC is less highly poised for forward synthesis at stall positions, and background G44 synthesis is not a problem for kinetic analysis, using a 100 μM ATP pulse. Using a 10 μM ATP pulse, however, in the presence of both TFIIF and TFIIS, resulted in a higher proportion of backtracked and cleaved ECs (data not shown), so 100 μM ATP was selected for experiments with both TFIIF and TFIIS.

In Figure 4, sample gel data are shown, obtained in the presence of TFIIF and in the presence of TFIIF+TFIIS. This qualitative comparison suggests the following conclusions: (1) TFIIF causes RNAP II to advance beyond stall positions by scavenging trace ATP or GTP and/or misincorporation of AMP for GMP; (2) TFIIS stimulates nascent RNA dinucleotide cleavage; (3) TFIIF permits transient RNAP II pausing at the A43 stall position without evidence for stimulation of RNA cleavage; and (4) TFIIS suppresses transient pausing. The first point is discussed above (Figure 3). TFIIS stimulates dinucleotide cleavage from C40→U38 and from A43→A41, as previously shown by others and by us.[3,14,16,17,35] Notice the presence of the A41 and U38 gel bands in the presence of TFIIS (Figures 3 and 4). In the presence of TFIIF alone, A41 originates from overrunning the C40 stop, not from dinucleotide cleavage from the A43 stall point. In the presence of TFIIF alone, U38 is not detected, because C40→U38 cleavage is not supported, in the absence of TFIIS. Transient pausing is observed in the presence of TFIIF. Pausing is indicated by the failure of ECs to advance significantly from A43 in the time span from 0.1 to 0.5 second. Paused (or backtracked and cleaved) A43 ECs advance with longer elongation times (see Figure 5). The extent of backtracking in

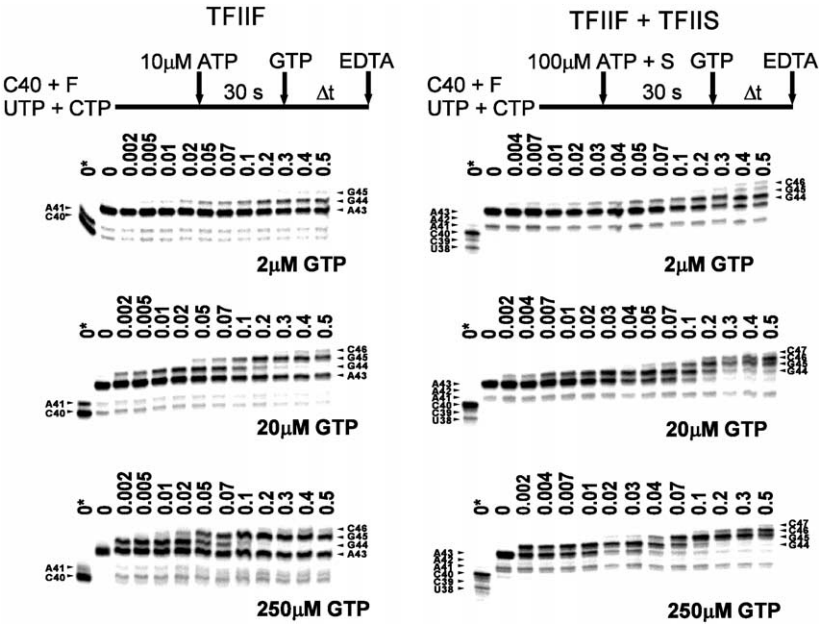

Figure 4. Elongation in the presence of TFIIF (left panels) and TFIIF+TFIIS (right panels). Protocols are shown above gel data. Elongation data at 2, 20 and 250 μM GTP are shown. TFIIS (S) induces nascent RNA cleavage from C40→U38 and from A43→A41.[3] In the absence of TFIIS, TFIIF (F) stimulates incorporation of trace ATP at C40 to synthesize A41. 0* indicates no ATP pulse, no GTP chase. 0 indicates ATP pulse with no GTP chase. Times are indicated in seconds. Background incorporation of trace GMP at A43 (or misincorporation of AMP) to synthesize G44 (*A44) is acceptably low.

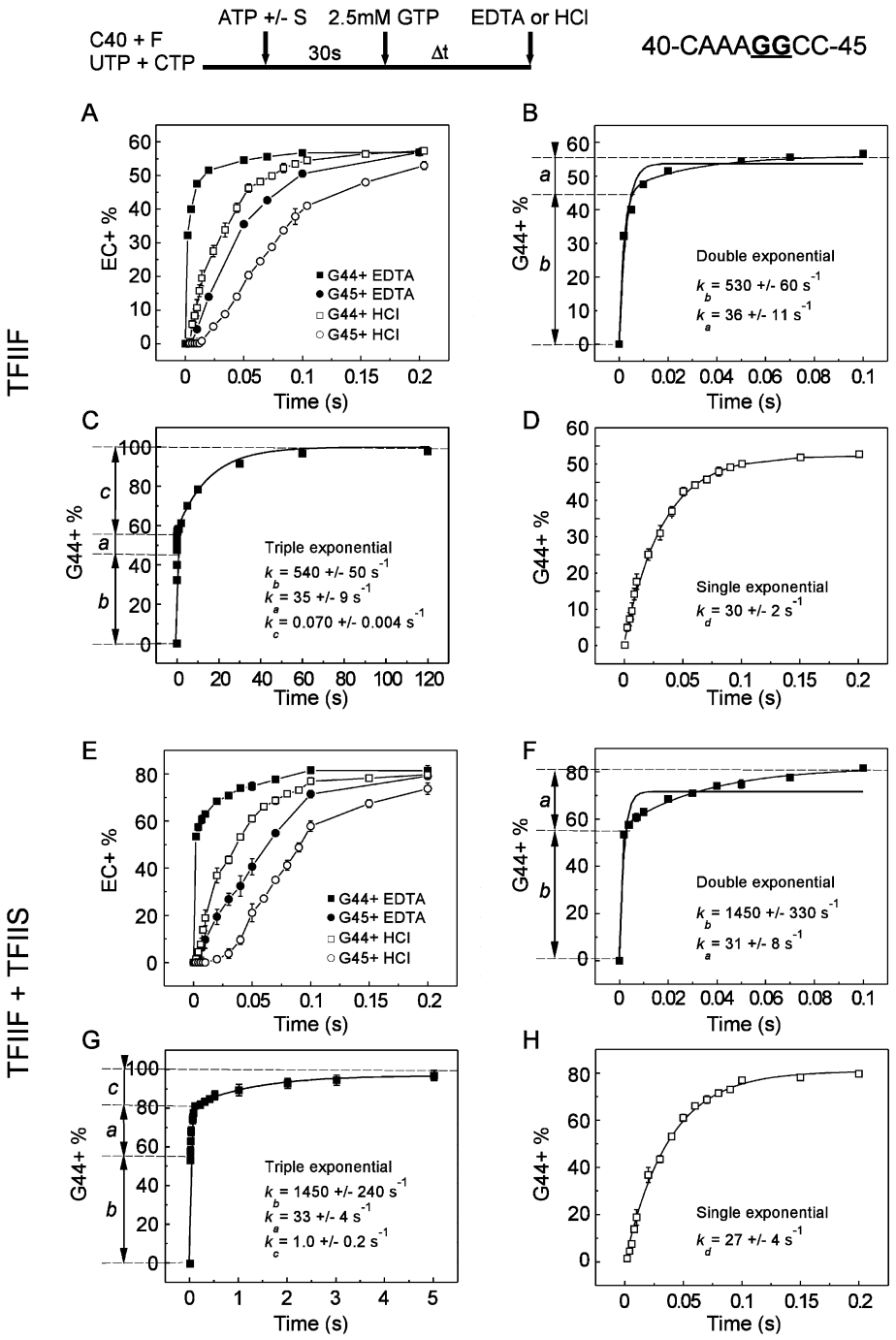

Figure 5. G44 and G45 synthesis at 2500 μM GTP. Double-quench protocol and model-independent analyses. A–D, TFIIF alone; E–H, TFIIF+TFIIS. A and E, Double-quench protocol indicating isomerization (EDTA quench) and chemistry (HCl quench). Filled symbols indicate EDTA quench data. Open symbols indicate HCl quench data. Symbols are uniform throughout the Figure. EC+% indicates G44 or G45+all longer transcripts, expressed as a percent. B, C, F and G, G44+% rate curves plotted with 0.1, 120 or 5 seconds time scales. Gray lines (B and F) represent the best fit to a single phase exponential, which is inadequate to fit the EDTA quench rate data. D and H, HCl quench data for G44 synthesis rates can be fit to a single exponential up to 0.2 second. All experiments were done in triplicate except the EDTA quench data for TFIIF alone, which was done once. Error bars indicate standard deviation. At some data points error bars are obscured by the graph symbol.

paused A43 ECs has not yet been determined, but with TFIIF as the sole elongation factor, the majority of transiently paused ECs are probably not backtracked beyond the pre-translocated state.[3] Transient pausing can occur without substantial backtracking,[3,32,33] and paused ECs demonstrate homogeneous kinetic behavior in forward elongation (Figure 5), indicating that a mixture of many paused conformations (i.e. many backtracked states) does not form during the brief duration of the stall. In the presence of TFIIS, paused ECs are not evident. With TFIIS addition, about 7% of A43

ECs advance slowly, but these ECs advance with similar kinetics to A41 ECs, which are the product of RNA cleavage from A43 (Figure 4, right panel; 250 μM GTP). There is clearly a period of conformational recovery for cleaved A41 ECs, because they are not rapidly extended in the presence of 100 μM ATP. If transcriptional restart were rapid, little A41 would be apparent in the gels, because 100 μM ATP supports rapid A42 and A43 synthesis for active pathway ECs. We conclude that, in the presence of TFIIS, transient pausing is suppressed, and paused ECs either quickly re-enter active synthesis or are backtracked to cleave a dinucleotide and restart elongation from A41. Some A43 ECs may progress through recovery without cleavage to A41, but, if this is the case, these ECs advance with very similar kinetics to A43 ECs that are first cleaved to A41 before recovery and restart. In the presence of TFIIS, at most 7% of A43 ECs could be in a paused conformation.[3] In the presence of TFIIF alone, almost 50% of A43 ECs are paused. We conclude that TFIIS suppresses transient transcriptional pausing.

Double-quench protocol distinguishes active site isomerization from chemistry

Cameron and colleagues determined that, in the presence of Mn^{2+} as the metal co-factor, isomerization and chemistry could be distinguished as separate stages for poliovirus RNA-dependent RNAP-catalyzed elongation, using EDTA quenching to detect isomerization and HCl quenching to determine chemistry.[6,7] We, therefore, tested both EDTA and HCl as quenching agents of the human RNAP II elongation reaction (Figure 5). As previously demonstrated for poliovirus RNAP, human RNAP II can protect active site divalent cations from EDTA chelation, in an isomerization step prior to chemistry. Quenching with EDTA indicates sequestration of the active site Mg^{2+} atoms. Chemistry occurs subsequently, as shown from HCl quench curves. The isomerization step must be essentially irreversible, because the EDTA quench curve is so well separated from the HCl quench curve. If isomerization were rapidly reversible, EDTA and HCl quench rate curves would superimpose. To simplify the kinetic analysis of the EDTA quench curves, we assume that the isomerization step is irreversible, but this must be a reasonable assumption for the reason cited above.

Model-independent analyses

Model-independent analysis is used to gain a simplified view of the elongation mechanism, as a prelude to global kinetic analysis.[28,36] The goal of model-independent analysis is to determine the number, amplitudes and apparent rates of different kinetic phases of a reaction. As the substrate GTP is increased, apparent rates approach true rate constants for elemental reaction steps, so the model-independent analysis at high GTP may be particularly informative for construction of an adequate global kinetic model. Model-independent analyses are shown in Figure 5 for the reaction stimulated by TFIIF or TFIIF+TFIIS at 2500 μM GTP. In Figure 6, we show global kinetic analyses for synthesis of the G44 and G45 bonds, determined at multiple GTP concentrations. In Figure 7, we show inferred reaction mechanisms and rate constants, derived from the kinetic analyses in Figures 5 and 6. The rate curve simulations shown in Figure 6 derive from the kinetic mechanisms shown in Figure 7.

For the experiments shown in Figure 5, reactions were quenched either with EDTA or HCl. In Figure 5(A and E), EDTA and HCl quench rate curves are compared for G44 and G45 synthesis. Separation of isomerization (EDTA quench) and chemistry (HCl quench) rate curves indicates a smooth cadence between A43 isomerization and G44 chemistry and subsequent G44 isomerization and G45 chemistry. Separation of EDTA and HCl quench curves indicates that additional rate-limiting steps may separate initial, essentially irreversible A43 isomerization and subsequent G44 chemistry. From the known steps of the RNAP II elongation mechanism, additional steps must separate G44 chemistry and G44 isomerization, including GTP-loading into the RNAP II active site, translocation, and pyrophosphate release.

When elongation times up to 0.1 second are considered for EDTA quench data (Figure 5B and F), kinetic parameters for the fastest phases of the RNAP II elongation mechanism can be estimated. In this short time interval, G44 synthesis rate curves (EDTA quench) can be fit adequately to double exponential curves (black curves) but not single exponential curves (gray curves), indicating at least two distinct rapid phases of the elongation reaction from A43. The rates are tabulated in the Figures, and the corresponding fractions (*b* and *a*) are indicated, as vertical arrows on the G44+% scale. Fractions *b*, *a* and *c* represent the estimated occupancies of the A43*b* (post-translocated) A43*a* (pre-translocated) and A43*c* (paused or backtracked and cleaved) EC conformations (Figure 7). The three distinct reaction rates (k_b, k_a, and k_c) ascribed to these different EC conformations are well-resolved in the model-independent analyses shown in Figure 5. The existence of at least two rapid reaction phases is confirmed by studies with α-amanitin, because the fastest reaction phase (*b*) is found to be α-amanitin-resistant, but the slower reaction phase (*a*) is sensitive.[29]

Because the two rate phases are not merged into a single rate at high GTP concentration, the two rate phases represent distinct conformations of the A43 EC (A43*b* and A43*a*) that respond to addition of GTP substrate in distinct ways. If the two reaction phases were merged into a single rate at high GTP concentration, this would indicate a reaction mechanism in which a single conformation of the EC could diverge into two distinct elongation pathways. Biphasic rate curves describing elongation by

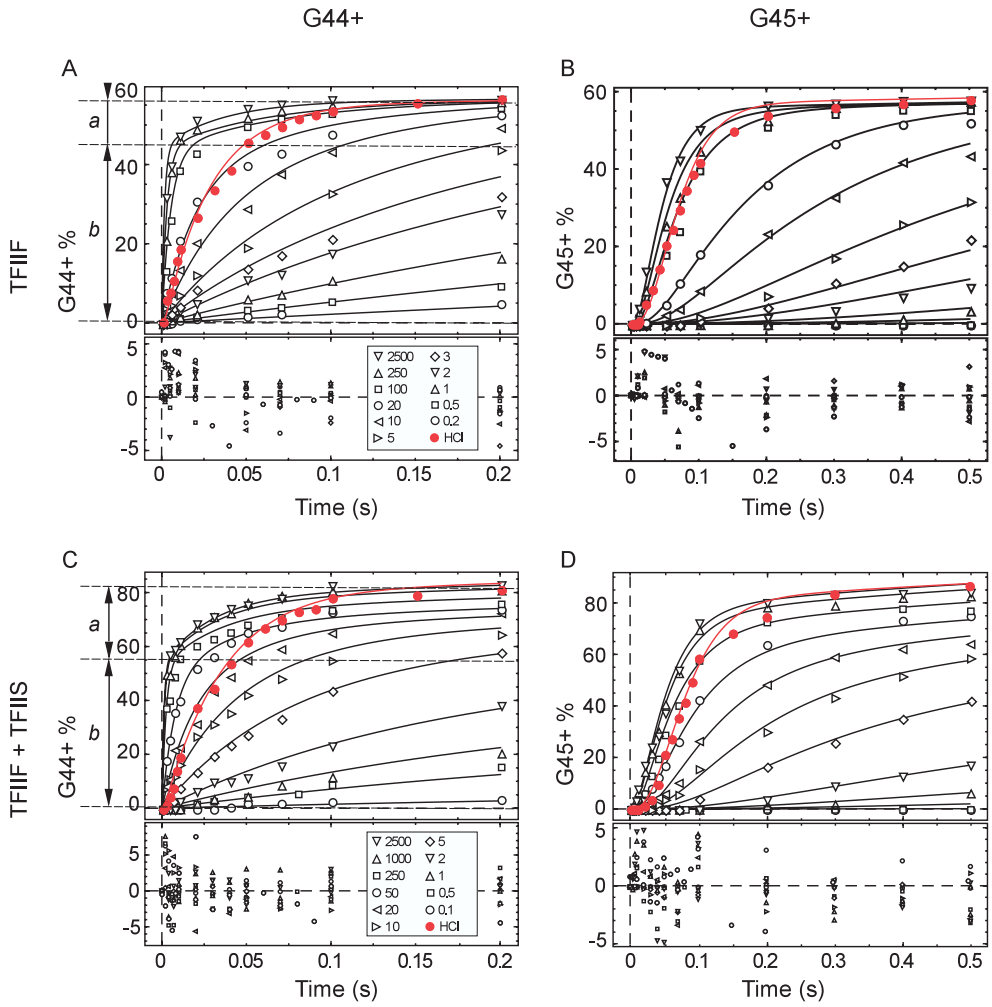

Figure 6. Global kinetic analyses of elongation by RNAP II in the presence of TFIIF (A and B) and TFIIF + TFIIS (C and D). A and C, G44 synthesis rates. B and D, G45 synthesis rates. GTP concentrations were tested between 0.1 and 2500 μM, as indicated in the keys. Reactions were quenched with EDTA (black) or HCl (red). For HCl quench rate curves, the GTP concentration was 2500 μM. Residuals, a statistical test, are shown below, indicating the quality of curve fits to experimental data. The kinetic models used for curve fitting are shown in Figure 7.

E. coli RNAP were interpreted in terms of this second type of mechanism, in which a single starting conformation diverges into two forward pathways.[26] The rate data for human RNAP II, however, cannot be fit using this type of model. Instead, there appear to be at least two distinct forms of the active pathway RNAP II EC at the A43 stall position (post- and pre-translocated) with different elongation kinetics to G44.

When the EDTA quench reaction is analyzed through longer times (120 or 5 seconds), paused (TFIIF alone) and cleaved (TFIIF + TFIIS) ECs advance, providing best estimates of the rates forward for the slowest conformations of the EC. Rate plots to 120 or 5 seconds must be fit with well-resolved triple exponential curves, indicating a minimum of three conformations of the RNAP II EC at the A43 stall point: two that elongate rapidly (A43*b*, A43*a*) and one that advances much more slowly (A43*c*). The two most rapid elongation phases have different responsiveness to GTP substrate, but the slowest phase is largely unresponsive to GTP, indicating that a conformational change (escape from pausing) is required for these ECs to re-enter the active elongation pathway.

With TFIIF as the sole elongation factor, the fastest phase of the triple exponential has a fractional occupancy of about 45% of total ECs and an apparent rate of 540($\pm$50) s^{-1} (Figure 5B; fraction *b*). The fastest reaction phase is too fast to measure with confidence using the RQF-3, for which the fastest start–stop time is 0.002 second. As a result of instrument limitation, only a few data points can be collected (at 25 °C) that relate to the fastest RNAP II reaction rate. So 540 s^{-1} is probably a minimal estimate of the true rate constant. The next fastest reaction phase (fraction *a*) has a fractional occupancy of about 11% of total ECs and an apparent rate of 35($\pm$9) s^{-1}. This slower rate is accurately measured with the RQF-3. In the presence of TFIIF as the sole stimulatory elongation factor, only about 56% of ECs are initially on the forward elongation pathway. The remaining 44% of total ECs are paused (fraction *c*) and extend slowly at a rate of 0.07($\pm$0.004) s^{-1}.

In the presence of TFIIF + TFIIS, the triple

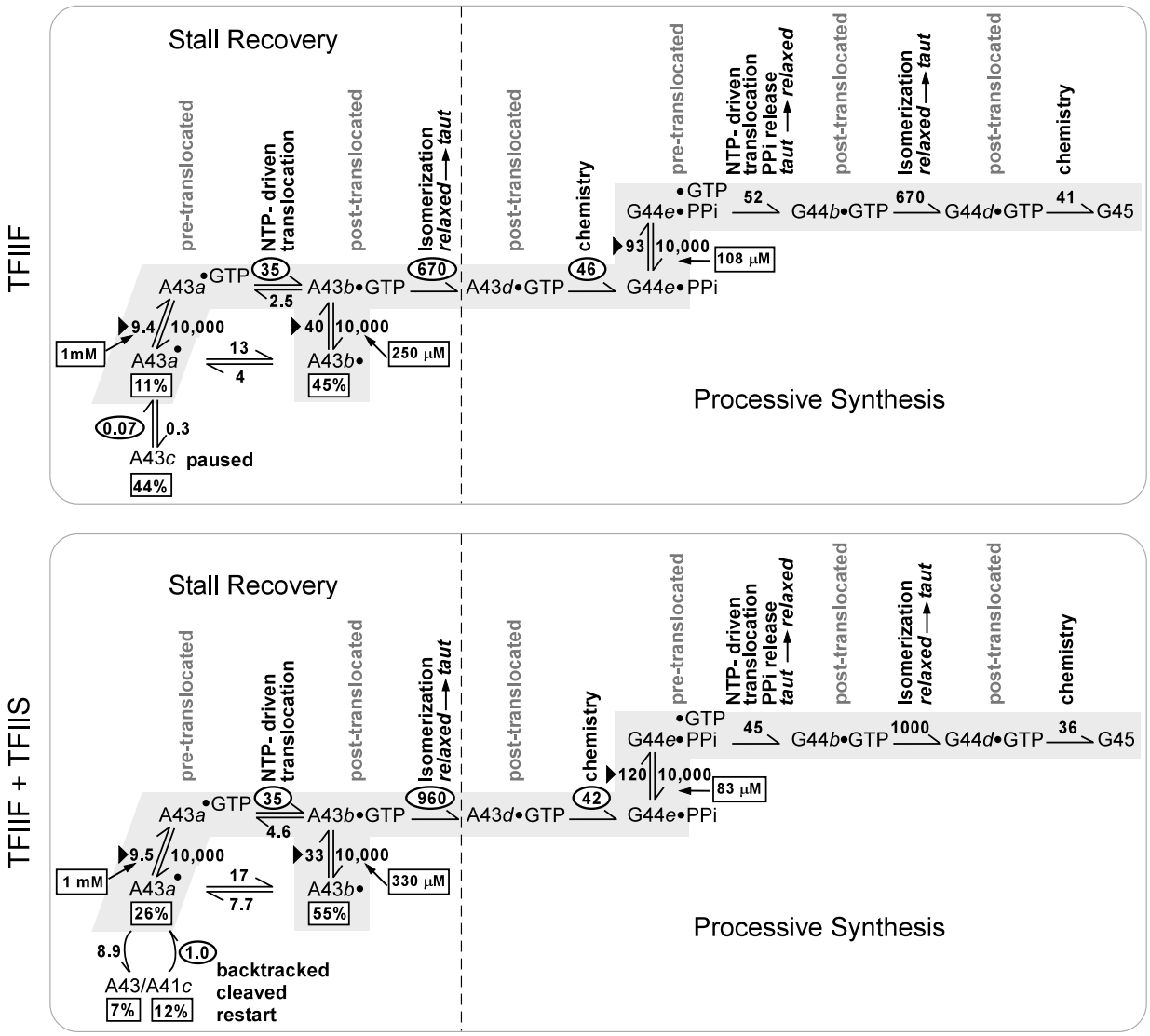

Figure 7. Adequate kinetic models to describe RNAP II elongation stimulated by TFIIF and TFIIF+TFIIS. Rate constants for GTP-dependent steps are in units of $\mu M^{-1}\,s^{-1}$ (steps indicated with black triangles). Estimated K_ds for GTP binding are also indicated. GTP-independent rate constants have units of s^{-1}. Lower case italic letters (*a*, *b*, *c*, *d*, and *e*) indicate distinct conformational states of the EC. Fractions (A43*a*, A43*b*, and A43*c*) indicated from model-independent analyses (Figure 5) are boxed. Rate constants (from apparent rates k_a, k_b, k_c, and k_d) indicated from model-independent analyses are within ovals. Black dots indicate whether the cognate DNA template base projects toward the main RNAP II channel (pre-translocated EC) or the secondary pore (post-translocated EC) (see Figure 1). Main pathways for elongation are shaded gray. PPi indicates pyrophosphate. Relaxed and taut transitions are between closed (EDTA-resistant) and open (EDTA-sensitive) conformations of the EC (Figure 1).

exponential indicates a fastest reaction phase with a fractional occupancy of about 55% of total ECs and an apparent rate of 1450($\pm$240) s^{-1} (Figure 5G; fraction *b*). The next fastest reaction phase (fraction *a*) has a fractional occupancy of about 26% of total ECs and an apparent rate of 33($\pm$4) s^{-1}. So in the presence of both TFIIF and TFIIS, about 81% of total ECs are extended within 0.1 second, indicating that these ECs are on the forward elongation pathway. We attribute the 25% increase in rapidly elongating ECs that accompanies addition of TFIIS to suppression of transcriptional pausing by TFIIS. In the presence of TFIIS, most of the remaining 19% of total ECs (fraction *c*) are not paused but are in the backtracked, cleaved and restart pathway. About 7% of A43 ECs are very slow to advance.[3] These ECs are expected to be backtracked and poised for dinucleotide cleavage to A41, although some of these ECs may recover at the A43 position without cleavage. Cleaved A41 ECs extend slowly.[3] A43 and A41 ECs that are in the backtracking (cleavage) and recovery pathway elongate with an apparent rate of 1.0($\pm$0.2) s^{-1}, similar to the determination made previously.[3] Therefore, the major differences between the mechanism stimulated by TFIIF alone and TFIIF+TFIIS involves TFIIS activities in suppression of transcriptional pausing and in supporting RNA cleavage, recovery and restart. The apparent rates that we measure at 2500 μM GTP are expected to approach elemental rate constants in a global kinetic analysis.

HCl quench data specify the time of chemistry.

With EDTA quenching, if Mg^{2+} atoms are sequestered in a tightened active site, elongation can continue forward after EDTA addition. In principle, the reaction could reverse after addition of EDTA, but, in studies of the forward elongation reaction, reversal of isomerization is not detected. With HCl addition, the reaction is quenched instantly. In Figure 5D and H, rate data for G44 chemistry are fit to single phase exponential curves, with rates of $k_d = 30(\pm 2)\ s^{-1}$ (TFIIF) and $k_d = 27(\pm 4)\ s^{-1}$ (TFIIF + TFIIS). When HCl quench curves are analyzed to longer times, the slowest rate of elongation (k_c) is confirmed (not shown). HCl quench rate data appears monophasic rather than biphasic in the 0.2 second time span, because the rate of chemistry is too slow to resolve the two previous isomerization rates, detected in the EDTA quench rate data (Figure 5B and F).

Based on the model-independent analyses, it was our judgement that the EDTA quench data were most informative about NTP-dependent steps in the RNAP II mechanism. EDTA quenching allows faster kinetic events to be analyzed than HCl quenching. EDTA quenching yields higher kinetic complexity than HCl quenching, indicating that analysis based on HCl quench data alone would oversimplify the RNAP II mechanism. The higher kinetic complexity reflected in the EDTA quench data is confirmed by inhibition studies using α-amanitin, which distinguishes two translocation states of RNAP II,[29] as indicated in EDTA quench rate curves. Furthermore, active site isomerization requires prior NTP loading, so EDTA quench data were considered to better reflect substrate NTP binding events than HCl quench data, which stop the reaction at a later stage of elongation.

Global kinetic analyses

To simulate the most rapid rates of RNAP II elongation, transcription was monitored through both the G44 and G45 bond positions through 0.2 and 0.5 second, using the running start, two-bond, double quench protocol (Figure 6). Curve fitting was done with the program DYNAFIT,[37] using the pathway and rate constants shown in Figure 7. In designing the simulation shown in Figure 7, every attempt was made to preserve the estimations of rate constants from apparent rates (k_a, k_b, k_c, and k_d) and corresponding EC fractions (*a*, *b*, *c*) derived from the model-independent analyses at 2.5 mM GTP (Figure 5). In the discussion that follows, different EC conformations (*a*, *b*, *c*, *d*, and *e*) are described according to the notations defined in Figure 7. EDTA quench rate curves are shown for GTP concentrations from 0.1 to 2500 μM.

HCl quench rate curves are shown for 2500 μM GTP only, because steps between isomerization and chemistry were not thought to be highly NTP-dependent, and the HCl quench defines the chemical step of the reaction. Also, the 40-CAAA**GG**CCTTT-50 template is not optimal for determining NTP-dependent effects on the rates of chemistry, because it encodes incorporation of GMP at both the G44 and G45 positions. In the future, we will test templates with 44-**GC**-45, 44-**GT**-45 and/or 44-**GA**-45 sequences, to determine the effects of CTP, UTP and ATP on G44 synthesis. The 44-**GG**-45 template is useful for the current study, because for this template NTP competition is minimized at the G44 position in the two-bond assay. A43*b* + GTP → A43*b*.GTP is very rapid, followed by rapid A43*b*.GTP → A43*d*.GTP isomerization (both steps are essentially complete in 0.002 second), and A43*d*.GTP → G44*e*.PPi chemistry is slow (rate of about $k_d \sim 30\ s^{-1}$), so EDTA quench curves provide the most recent reporting about NTP-binding steps.

Global analyses are shown for RNAP II elongation in the presence of TFIIF and in the presence of both TFIIF and TFIIS, to assess effects of TFIIS on forward synthesis and to gain insight into the RNAP II elongation mechanism stimulated by TFIIF. At higher GTP concentrations (20 to 2500 μM), EDTA quench rate curves for G44 synthesis are notably biphasic (Figure 6A and C), as was also demonstrated in the model-independent analyses (Figure 5B and F). In the HCl quench data, these two kinetic phases merge into a single detectable rate, because of the delay between initial rapid isomerization and chemistry (Figure 5A, D, E and H).

EDTA quench G45 synthesis rate curves (Figures 5A and E and 6B and D) are sigmoidal in shape, indicating a rate-limiting step prior to G44 isomerization. In part, this sigmoidal character can be attributed to a slow rate of G44 chemistry (or an undefined isomerization step preceding chemistry) ($k_d = 30(\pm 2)\ s^{-1}$ or $k_d = 27(\pm 4)\ s^{-1}$; Figure 5D and H; HCl quench data). Translocation must separate G44 chemistry and G44*b*.GTP → G44*d*.GTP isomerization, and translocation is expected to be rate-limiting in this interval. A43*a*.GTP → A43*b*.GTP translocation proceeds at a rate of $k_a = 35(\pm 9)\ s^{-1}$ or $k_a = 33(\pm 4)\ s^{-1}$ (Figure 5C and G). The mechanism shown in Figure 7 couples pyrophosphate release to NTP-driven translocation, so G44*e*.PPi.GTP → G44*b*.GTP translocation and coupled pyrophosphate release is expected to be a rate-limiting step, proceeding at a rate of about $k_d \sim 30\ s^{-1}$. G44*b*.GTP → G44*d*.GTP isomerization is expected to be very rapid, because A43*b* + GTP → A43*b*.GTP → A43*d*.GTP proceeds at a rate of about $k_b = 540\ s^{-1}$ or $k_b = 1450\ s^{-1}$ (Figure 5C and G). As shown for the HCl quench data, G45 synthesis is a slow step after G44*d*.GTP isomerization. Based on the rate of A43*d*.GTP → G44*e*.PPi chemistry, this rate constant should be approximately $k_d \sim 30\ s^{-1}$.

Homogeneous kinetic behavior of the RNAP II EC preparation

Because RNAP II ECs are isolated from an extract of HeLa nuclei, by a Sarkosyl and salt-washing procedure, the biochemical composition of the EC preparation is not known. It was therefore

important to establish that our kinetic measurements reflected intrinsic functions of RNAP II elongation rather than different activities of a mixture of biochemically heterogeneous ECs with distinct kinetic behavior. Based on the stringency of the washing procedure, we were confident that endogenous TFIIF, TFIIS and general RNAP II initiation factors would dissociate from washed ECs,[38] but more tightly bound factors might remain associated. Using the EDTA quench procedure for G44 synthesis indicated three conformations of the RNAP II EC, interpreted as pre-translocated, post-translocated and paused A43 ECs (or backtracked and cleaved) (A43*a*, A43*b* and A43*c*), but kinetic heterogeneity in G44 synthesis (Figure 5B, C, F and G) might be attributed to biochemical heterogeneity. From the HCl quench data (Figure 5D and H), however, it is unlikely that the pre- and post-translocated ECs detected in the EDTA quench data can be attributed to biochemical heterogeneity in the EC preparation. The two most rapid kinetic phases (*b* and *a*) merge into a single kinetic phase in the HCl quench rate data. Furthermore, the extent of pausing is regulated by addition of recombinant human TFIIS to the reaction, so occupancy of the slowest kinetic state (*c*) is determined, not by the EC preparation, but by treatments after purification: addition or omission of TFIIS.

Discussion

Translocation and the catalytic mechanism of human RNAP II

A compelling debate has been joined in the transcription and replication fields to clarify the mechanisms of translocation by multisubunit and simpler RNAPs and DNAPs. Landick[39] framed this debate in terms of the Brownian, thermal ratchet mechanism, in which translocation must precede NTP binding, and various "powerstroke" models, in which a protein conformational change drives forward translocation.[40] In the case of T7 RNAP, the powerstroke appears to be rotation of the O-α-helix, driven by templated NTP substrate binding to the NTP "pre-insertion" site.[41,42] Subsequent O-helix rotation and NTP movement into the T7 RNAP catalytic site tightens the active center for chemistry, providing the final induced fit conformational change that boosts fidelity of simple RNAPs and DNAPs.[41,43,44] After chemistry, pyrophosphate release is suggested to initiate relaxation of the T7 RNAP active site, rotating the O-helix against the DNA template to drive the next increment of translocation.[41] In this way, pyrophosphate release may be coupled to translocation, followed by NTP loading to the pre-insertion site, O-helix rotation, active site tightening and chemistry.

For yeast RNAP II, the powerstroke may involve bending or local unwinding of the bridge α-helix toward the RNA–DNA hybrid, as suggested by Kornberg and colleagues.[19,24,26] In support of a powerstroke model, our kinetic data for human RNAP II are inconsistent with a pure thermal ratchet mechanism because the kinetic analysis requires NTP binding to both pre- and post-translocated A43 ECs. On the other hand, the model does allow conversion between pre- and post-translocated ECs, in the absence of the templated GTP at the A43 stall position, as required by the Brownian ratchet mechanism. In our kinetic mechanisms, however, NTP-driven translocation must be significantly faster than the NTP-independent pathway. We posit that, during processive RNA synthesis, translocation is NTP-driven, consistent with an NTP-driven powerstroke mechanism. Loading of the NTP-dNMP base-pair from the main enzyme channel into the RNAP II active site could induce bridge α-helix bending or an alternate assisting protein conformational change. The conformational change would drive translocation by propelling the RNA–DNA hybrid and DNA duplex through the RNAP II main channel.

After NTP-driven translocation, the RNAP II EC isomerizes very rapidly (within 0.002 second; $k_b \sim 500$ to $1000\ s^{-1}$) to sequester the two active site Mg^{2+} atoms from EDTA chelation. Phosphodiester bond synthesis, however, occurs slowly ($k_d \sim 30\ s^{-1}$) after rapid isomerization ($k_b \sim 500$ to $1000\ s^{-1}$). This result could indicate that the chemical step is slow or that a slow isomerization step (or steps) separates initial rapid isomerization and chemistry. Very similarly, Tsai and colleagues have identified the chemical step as rate-limiting for elongation catalyzed by rat DNAP β.[36,45] Because the RNAP II active site tightens before chemistry, it must relax after chemistry, as observed in simple RNAP and DNAP mechanisms.[41,43,44] Here, we support a model in which the incoming NTP substrate helps to complete the previous bond addition cycle.[5] NTP-driven translocation, therefore, may be coupled to conformational relaxation of the RNAP II EC after chemistry, driving pyrophosphate release. Coupling of NTP-driven translocation to pyrophosphate release requires that a conformationally tightened RNAP II active site, at the time of chemistry, must relax after chemistry to complete each bond addition cycle and release pyrophosphate. The slow rate of NTP-driven translocation (G44*e*.PPi.GTP → G44*b*.GTP; $k \sim 52$ or $45\ s^{-1}$; Figure 7) is rate-limiting between G44 chemistry and G44 isomerization. We posit that NTP-driven translocation is coupled to a conformational change in the RNAP II EC. This conformational change allows subsequent pyrophosphate release.

Transient state kinetic analysis of RNAP II elongation

Our transient state kinetic analysis of human RNAP II elongation has several notable features. We utilized a running start, two-bond, double-quench protocol to obtain detailed insight into RNAP II

elongation. Using the running start, we stall RNAP II briefly before adding the next substrate NTP(s). To our knowledge, no other laboratories have reported complete transient state, multiple bond analyses of RNAPs or DNAPs, although, for our analyses, this treatment proved essential. We monitor the formation of at least two bonds because different kinetic information accrues from analysis of stall recovery (A43→G44) and processive synthesis (G44→G45). Analysis of a single bond would be less informative and potentially confusing. For G44 synthesis, after the stall at A43, the EDTA-quenching procedure produced biphasic rate curves in a 0.1 second time-course. HCl quenching, however, simplified the kinetics of G44 synthesis, indicating that the complexity of the EDTA quench curves provided detailed information about RNAP II translocation, a conclusion supported by studies with the translocation inhibitor α-amanitin.[29] Our analyses through two bonds, using the double quench procedure, provided us with rates that relate to different translocation states and to the timing of initial EC isomerization (EDTA quench) and chemistry (HCl quench). In this regard, rapid quench technology compares favorably with single-molecule elongation studies of *E. coli* RNAP, which only begin to approach single bond resolution.[32,33] A wide range of substrate GTP concentrations (0.1 or 0.2 to 2500 μM) was analyzed, taking many data points, to saturate the appropriate data space (Figure 6). This large collection of data, obtained using several elongation factors, provides the basis for our global kinetic analyses, which are consistent with our model-independent analyses. RNAP II has high conformational flexibility,[19,21] which makes the kinetic analysis particularly interesting and challenging. Furthermore, human RNAP II is highly responsive to regulators such as TFIIF and TFIIS, making analyses of biological significance.

Regulation by TFIIF and TFIIS

The view of TFIIF and TFIIS regulation of RNAP II that we present, based on transient state kinetic studies, is different from that previously inferred from steady-state approaches. We show that TFIIF accelerates RNAP II elongation rate by supporting the post-translocated EC, and TFIIS improves elongation efficiency by suppressing transcriptional pausing. By itself, TFIIS does not accelerate elongation rate nor does it enhance rate when combined with TFIIF over the rate supported by TFIIF alone. In the presence of both TFIIF and TFIIS, these factors appear to affect elongation independently, but inclusion of the two factors has a combinatorial effect on suppression of transient RNAP II pausing,[3] because of the cooperative nature of the independent actions of TFIIF and TFIIS. We show that, in order for TFIIS to have a strongly stimulatory effect on forward elongation, TFIIF must be present. Our explanation of these observations is as follows. TFIIS suppresses pausing whether or not TFIIF is present in the reaction, but in the absence of TFIIF, TFIIS supports entry of RNAP II into the backtracking, RNA cleavage and restart pathway. We suggest that the paused state of the EC is suppressed by TFIIS, because TFIIS accelerates rates into and out of the paused EC,[3] TFIIS may stimulate backtracking and TFIIS participates directly in RNA cleavage.[18] After cleavage of the nascent RNA, the EC must recover to commence RNA synthesis, but in the presence of TFIIS as the sole factor, the recovering EC may be more likely to enter another cycle of backtracking and cleavage rather than transcriptional restart. In the presence of both TFIIF and TFIIS, however, TFIIF compels RNAP II toward the post-translocated EC, so fewer ECs become trapped down the pausing, backtracking and RNA cleavage pathway. Suppression of pausing by TFIIS allows TFIIF to more efficiently stimulate the forward elongation mechanism. So TFIIF stimulates elongation by supporting the post-translocated EC. Elmendorf *et al*. demonstrated that TFIIF and TFIIS could interact to suppress the transcript cleavage activity of TFIIS.[46] We suggest that TFIIF has this effect by maintaining the post-translocated EC. TFIIS aids elongation by suppressing transcriptional pausing without noticeable stimulation of elongation rate, unless TFIIF or another stimulatory factor is also present. From a practical point of view, inclusion of TFIIS significantly enhances the efficiency of forward elongation from the A43 stall position, improving the kinetic analysis of rapid elongation by human RNAP II stimulated by TFIIF.

NTP substrate loading and NTP-driven translocation

As discussed in Introduction, we previously proposed a model for NTP-driven translocation by human RNAP II (Figure 1).[5] Analyses described here are fully consistent with the NTP-driven translocation model. These studies indicate that step-wise translocation of the RNA–DNA hybrid and DNA template through the RNAP II main channel is normally driven by prior binding of the substrate NTP to its cognate DNA base. Indeed, three unpaired DNA bases ($n+1$, $n+2$ and $n+3$; n=RNA length) face the main enzyme channel in the pre-translocated yeast RNAP II EC.[19] After pairing of the incoming NTP, the dNMP-NTP base-pair is thought to drive RNA–DNA hybrid displacement, allowing the substrate NTP to be loaded as a base-pair into the RNAP II active site for chemistry.

The reaction simulation shown in Figure 7 is not a perfect representation of the NTP-driven translocation model, because the scheme shown does not allow for base-pairing of the GTP substrate for G45 synthesis prior to G44 chemistry. This omission does not affect the quality of the data fit, however, because the GTP loading step is only rate-limiting at low GTP concentrations, at which the mechanism proceeds essentially as shown. At higher GTP

concentrations, NTP-driven translocation is rate-limiting, as shown in the mechanism.

Combining the NTP-driven translocation model and the yeast RNAP II structure, it appears that substrate NTPs are normally loaded through the main enzyme channel rather than through the secondary pore, because prior DNA translocation appears to be required for secondary pore NTP loading (Figure 1).[20] On the basis of structural data, others have suggested that the secondary pore is the primary route for NTP loading.[19,21,24,27,47] Our kinetic studies, however, indicate that this inference may not be correct. Of course, to the post-translocated EC, NTPs would be expected to load through the secondary pore,[20] so, in our experiment, the A43*b* EC might load GTP through the secondary pore. A43*a* and G44*e* are expected to load GTP through the main channel. During processive synthesis, NTPs are expected to load through the main RNAP II channel, prior to the translocation step. So, secondary pore loading of an NTP substrate is expected only after transcriptional stalling and NTP-independent translocation, which for human RNAP II is highly dependent on stimulation by an elongation factor such as TFIIF.

Materials and Methods

Cell culture, extracts and proteins

HeLa cells were purchased from the National Cell Culture Center (Minneapolis, MN). Extracts of HeLa cell nuclei were prepared as described.[48] Recombinant TFIIF was prepared as described.[49,50] Recombinant human TFIIS was purified by phosphocellulose chromatography followed by MonoS chromatography (our unpublished procedure).

NTP stocks

Ultrapure NTP sets were purchased from Amersham Pharmacia Inc. Based on our experience using these reagents, CTP and UTP stocks appear to be free of detectable ATP and GTP contamination. The ATP stock is substantially free of GTP contamination. The GTP preparation appears to be lightly contaminated with ATP, which does not complicate our experiment, because GTP is the final addition to the reaction, after prior addition of ATP. In reactions containing TFIIF, we observe some tendency to incorporate AMP or GMP, when none has been deliberately added to the reaction. As we show here, this observation results from stimulation of RNAP II elongation by TFIIF. The probable major source of ATP and GTP contamination in these reactions is the HeLa extract from which we initially derive ECs and not the NTP stocks. When TFIIS is added to the reaction in addition to TFIIF, inappropriate AMP and GMP incorporation is suppressed, indicating that the TFIIF preparation is not likely to be a source of ATP or GTP contamination.

Preparation of RNAP II ECs

Protocols for rapid quench-flow experiments have been published.[3,4,5,13] Briefly, ^{32}P-labeled C40 (40-nucleotide RNA ending in a 3′-CMP) RNAP II ECs were formed on metal bead-immobilized templates in a HeLa transcription extract. Initiation was from the adenovirus major late promoter using a modified downstream sequence (+1-ACTCTCTTCCCCTTCTCTTTCCTTCTCTTCCCTCTCC TCC-+40). The purpose of the 39-nucleotide CT-cassette is to synthesize C40 with ApC dinucleotide, dATP, [α-^{32}P]CTP and UTP, bypassing the requirement for addition of ATP and GTP. C40 ECs were washed with 1% Sarkosyl and 0.5 M KCl buffer to dissociate initiation, elongation, pausing and termination factors, contributed by the HeLa extract, and re-equilibrated with transcription buffer containing 8 mM $MgCl_2$ and 20 μM CTP and UTP. TFIIF (10 pmol per 15 μl reaction) and TFIIS (3 pmol per reaction) were added as indicated in particular protocols. In work to be published elsewhere, we have determined that Sarkosyl-washed RNAP II ECs behave very similarly to ECs prepared by washing in 60 mM or 1 M KCl transcription buffer, supporting the use of Sarkosyl-washed ECs to analyze human RNAP II elongation.

Running start, two-bond, double-quench protocol

The running start, two-bond protocol has been described.[3,4,5,13] Here, we improve the procedure by reporting data from experiments quenched with EDTA or with HCl.[6,7] Rapid quench experiments were done using the Kintek Rapid Chemical Quench-Flow (RQF-3) instrument. All steps were done at 25 °C. Elongation was through the sequence 40-CAAAGGCC-47. C40 ECs were incubated with 20 μM CTP and UTP. 10 or 100 μM ATP (depending on the protocol) was added to bead-immobilized C40 ECs on the bench top, to extend the EC to the A43 position. During the next 30–120 seconds (depending on the protocol), ECs were loaded into the left sample port of the RQF-3 instrument. GTP (in transcription buffer) at twice its working concentration was loaded into the RQF-3 right sample port. Programmed, equal volume mixing in the RQF-3 first combined ECs with GTP substrate. Reactions were then quenched with 0.5 M EDTA or 1 M HCl, after a precisely timed delay (>0.002 second). For EDTA-quenched reactions, ECs on beads were collected with a magnetic particle separator and processed by electrophoresis, as described.[3–5,13] HCl quenching dissociates the transcript from the RNAP II EC. HCl-quenched reactions were delivered into collection tubes containing a sufficient volume of 1 M KOH and 300 mM Tris-base (~70 μl), to neutralize the pH of the solution. Beads were removed using a magnetic particle separator. The solution was extracted with an equal volume of phenol-chloroform. The aqueous phase was adjusted to 0.3 M sodium acetate containing 20 μg of glycogen carrier and ethanol-precipitated. After vacuum drying, RNA samples were analyzed by electrophoresis. Gel bands were quantified using a Molecular Dynamics Phosphorimager. At the A43 stall point, the EC fractionates into multiple conformational states, which are revealed by their distinct elongation kinetics to G44. Formation of the G44 bond, therefore, provides detailed insight into the mechanism and informs about recovery from the transcriptional stall at A43. The transition from G44→G45 provides information about processive elongation.

Model-independent analysis

Model-independent analysis[28,36] was done with the program Microcal Origin version 7.0, fitting rate data to

single, double or triple exponential rate curves, as appropriate. A significant advantage of the human RNAP II elongation system is that these kinetic phases are so easily distinguished, giving a clear demonstration of distinct rates, which relate to distinct conformations of the RNAP II EC at the time of substrate GTP addition. Typical reproducibility of experiments is demonstrated in Figure 5. The high reproducibility of quantification results from determining the signal within individual gel tracks. Because transcripts are labeled at multiple CMP positions near the 5′ end, and because signal is determined as a ratio of bands within a single gel lane, there is little contribution of error due to gel sample loading, and rate determinations are highly consistent in independent experiments. Independent experiments compared in Figure 5 were done over a period of eight months, during which period, the RQF-3 was serviced and re-calibrated.

Global kinetic modeling

Global kinetic modeling was done using the program DYNAFIT.[37] Model-independent analysis was used to make the best initial estimates of individual rate constants in the mechanism. Models were constrained to be initially in thermodynamic balance, and thermodynamic balance was required around cycles. For the reaction in the presence of TFIIF + TFIIS, the RNA cleavage and restart pathway cannot be brought into thermodynamic balance with the pre-translocated EC, maintaining an adequate curve fit (A43*a* ↔ A43/A41*c* is not in thermodynamic balance). Qualitatively, this observation indicates that, at low GTP concentration, A43 backtracking and cleavage is enhanced, a result we do not understand. A more detailed analysis of the backtracking, cleavage and restart pathway has been published elsewhere.[3] GTP dissociation rates were constrained to be 10,000 s^{-1}, although DYNAFIT would select faster rates. Estimated rate constants were selected so that the rate constants for G44 synthesis are as similar as possible to the rate constants for G45 synthesis. So far as we can determine, simpler models cannot describe the human RNAP II elongation mechanism.[5]

Acknowledgements

This work was supported by a grant from the National Institutes of Health (GM57461 to Z.F.B.). We thank Y. A. Nedialkov for help with preparation of the manuscript. Z.F.B. receives support from the Michigan State University Agricultural Experiment Station.

References

1. Johnson, K. A. (1995). Rapid quench kinetic analysis of polymerases, adenosinetriphosphatases, and enzyme intermediates. *Methods Enzymol.* **249**, 38–61.
2. Johnson, K. A. (1992). Transient-state kinetic analysis of enzyme reaction pathways. *Enzymes*, **20**, 1–61.
3. Zhang, C., Yan, H. & Burton, Z. F. (2003). Combinatorial control of human RNA polymerase II (RNAP II) pausing and transcript cleavage by transcription factor IIF. Hepatitis {delta} antigen, and stimulatory factor II. *J. Biol. Chem.* **278**, 50101–50111.
4. Nedialkov, Y. A., Gong, X. Q., Yamaguchi, Y., Handa, H. & Burton, Z. F. (2003). Transient state kinetics of RNA polymerase II elongation. *Methods Enzymol.* **371**, 252–262.
5. Nedialkov, Y. A., Gong, X. Q., Hovde, S. L., Yamaguchi, Y., Handa, H., Geiger, J. H. *et al.* (2003). NTP-driven translocation by human RNA polymerase II. *J. Biol. Chem.* **278**, 18303–18312.
6. Arnold, J. J. & Cameron, C. E. (2004). Poliovirus RNA-dependent RNA polymerase (3Dpol): pre-steady-state kinetic analysis of ribonucleotide incorporation in the presence of Mg^{2+}. *Biochemistry*, **43**, 5126–5137.
7. Arnold, J. J., Gohara, D. W. & Cameron, C. E. (2004). Poliovirus RNA-dependent RNA polymerase (3Dpol): pre-steady-state kinetic analysis of ribonucleotide incorporation in the presence of Mn^{2+}. *Biochemistry*, **43**, 5138–5148.
8. Bengal, E., Flores, O., Krauskopf, A., Reinberg, D. & Aloni, Y. (1991). Role of the mammalian transcription factors IIF, IIS, and IIX during elongation by RNA polymerase II. *Mol. Cell. Biol.* **11**, 1195–1206.
9. Izban, M. G. & Luse, D. S. (1992). Factor-stimulated RNA polymerase II transcribes at physiological elongation rates on naked DNA but very poorly on chromatin templates. *J. Biol. Chem.* **267**, 13647–13655.
10. Lei, L., Ren, D. & Burton, Z. F. (1999). The RAP74 subunit of human transcription factor IIF has similar roles in initiation and elongation. *Mol. Cell. Biol.* **19**, 8372–8382.
11. Renner, D. B., Yamaguchi, Y., Wada, T., Handa, H. & Price, D. H. (2001). A highly purified RNA polymerase II elongation control system. *J. Biol. Chem.* **276**, 42601–42609.
12. Tan, S., Aso, T., Conaway, R. C. & Conaway, J. W. (1994). Roles for both the RAP30 and RAP74 subunits of transcription factor IIF in transcription initiation and elongation by RNA polymerase II. *J. Biol. Chem.* **269**, 25684–25691.
13. Funk, J. D., Nedialkov, Y. A., Xu, D. & Burton, Z. F. (2002). A key role for the alpha 1 helix of human RAP74 in the initiation and elongation of RNA chains. *J. Biol. Chem.* **277**, 46998–47003.
14. Guo, H. & Price, D. H. (1993). Mechanism of DmS-II-mediated pause suppression by *Drosophila* RNA polymerase II. *J. Biol. Chem.* **268**, 18762–18770.
15. Izban, M. G. & Luse, D. S. (1992). The polymerase RNA II ternary complex cleaves the nascent transcript in a 3′–5′ direction in the presence of elongation factor SII. *Genes Dev.* **6**, 1342–1356.
16. Izban, M. G. & Luse, D. S. (1993). The increment of SII-facilitated transcript cleavage varies dramatically between elongation competent and incompetent RNA polymerase II ternary complexes. *J. Biol. Chem.* **268**, 12874–12885.
17. Gu, W. & Reines, D. (1995). Variation in the size of nascent RNA cleavage products as a function of transcript length and elongation competence. *J. Biol. Chem.* **270**, 30441–30447.
18. Kettenberger, H., Armache, K. J. & Cramer, P. (2003). Architecture of the RNA polymerase II-TFIIS complex and implications for mRNA cleavage. *Cell*, **114**, 347–357.
19. Gnatt, A. L., Cramer, P., Fu, J., Bushnell, D. A. & Kornberg, R. D. (2001). Structural basis of transcription: an RNA polymerase II elongation complex at 3.3 Å resolution. *Science*, **292**, 1876–1882.
20. Westover, K. D., Bushnell, D. A. & Kornberg, R. D.

(2004). Structural basis of transcription: separation of RNA from DNA by RNA polymerase II. *Science*, **303**, 1014–1016.
21. Cramer, P., Bushnell, D. A. & Kornberg, R. D. (2001). Structural basis of transcription: RNA polymerase II at 2.8 angstrom resolution. *Science*, **292**, 1863–1876.
22. Steitz, T. A. (1998). A mechanism for all polymerases. *Nature*, **391**, 231–232.
23. Steitz, T. A., Smerdon, S. J., Jager, J. & Joyce, C. M. (1994). A unified polymerase mechanism for non-homologous DNA and RNA polymerases. *Science*, **266**, 2022–2025.
24. Vassylyev, D. G., Sekine, S., Laptenko, O., Lee, J., Vassylyeva, M. N., Borukhov, S. & Yokoyama, S. (2002). Crystal structure of a bacterial RNA polymerase holoenzyme at 2.6 Å resolution. *Nature*, **417**, 712–719.
25. Sosunov, V., Sosunova, E., Mustaev, A., Bass, I., Nikiforov, V. & Goldfarb, A. (2003). Unified two-metal mechanism of RNA synthesis and degradation by RNA polymerase. *EMBO J.* **22**, 2234–2244.
26. Holmes, S. F. & Erie, D. A. (2003). Downstream DNA sequence effects on transcription elongation. Allosteric binding of nucleoside triphosphates facilitates translocation via a ratchet motion. *J. Biol. Chem.* **278**, 35597–35608.
27. Zhang, G., Campbell, E. A., Minakhin, L., Richter, C., Severinov, K. & Darst, S. A. (1999). Crystal structure of *Thermus aquaticus* core RNA polymerase at 3.3 Å resolution. *Cell*, **98**, 811–824.
28. Foster, J. E., Holmes, S. F. & Erie, D. A. (2001). Allosteric binding of nucleoside triphosphates to RNA polymerase regulates transcription elongation. *Cell*, **106**, 243–252.
29. Gong, X. Q., Nedialkov, Y. A. & Burton, Z. F. (2004). Alpha-amanitin blocks translocation by human RNA polymerase II. *J. Biol. Chem.* **279**, 27422–27427.
30. Bushnell, D. A., Cramer, P. & Kornberg, R. D. (2002). Structural basis of transcription: alpha-amanitin-RNA polymerase II cocrystal at 2.8 Å resolution. *Proc. Natl Acad. Sci. USA*, **99**, 1218–1222.
31. Palangat, M. & Landick, R. (2001). Roles of RNA:DNA hybrid stability, RNA structure, and active site conformation in pausing by human RNA polymerase II. *J. Mol. Biol.* **311**, 265–282.
32. Neuman, K. C., Abbondanzieri, E. A., Landick, R., Gelles, J. & Block, S. M. (2003). Ubiquitous transcriptional pausing is independent of RNA polymerase backtracking. *Cell*, **115**, 437–447.
33. Shaevitz, J. W., Abbondanzieri, E. A., Landick, R. & Block, S. M. (2003). Backtracking by single RNA polymerase molecules observed at near-base-pair resolution. *Nature*, **426**, 684–687.
34. Traut, T. W. (1994). Physiological concentrations of purines and pyrimidines. *Mol. Cell. Biochem.* **140**, 1–22.
35. Izban, M. G. & Luse, D. S. (1993). SII-facilitated transcript cleavage in RNA polymerase II complexes stalled early after initiation occurs in primarily dinucleotide increments. *J. Biol. Chem.* **268**, 12864–12873.
36. Dunlap, C. A. & Tsai, M. D. (2002). Use of 2-aminopurine and tryptophan fluorescence as probes in kinetic analyses of DNA polymerase Beta. *Biochemistry*, **41**, 11226–11235.
37. Kuzmic, P. (1996). Program DYNAFIT for the analysis of enzyme kinetic data: application to HIV proteinase. *Anal. Biochem.* **237**, 260–273.
38. Sopta, M., Carthew, R. W. & Greenblatt, J. (1985). Isolation of three proteins that bind to mammalian RNA polymerase II. *J. Biol. Chem.* **260**, 10353–10360.
39. Landick, R. (2004). Active-site dynamics in RNA polymerases. *Cell*, **116**, 351–353.
40. Wang, H. & Oster, G. (2002). Ratchets, power strokes, and molecular motors. *Appl. Phys. A*, **75**, 315–323.
41. Yin, Y. W. & Steitz, T. A. (2004). The structural mechanism of translocation and helicase activity in T7 RNA polymerase. *Cell*, **116**, 393–404.
42. Temiakov, D., Patlan, V., Anikin, M., McAllister, W. T., Yokoyama, S. & Vassylyev, D. G. (2004). Structural basis for substrate selection by T7 RNA polymerase. *Cell*, **116**, 381–391.
43. Johnson, S. J., Taylor, J. S. & Beese, L. S. (2003). Processive DNA synthesis observed in a polymerase crystal suggests a mechanism for the prevention of frameshift mutations. *Proc. Natl Acad. Sci. USA*, **100**, 3895–3900.
44. Doublie, S., Tabor, S., Long, A. M., Richardson, C. C. & Ellenberger, T. (1998). Crystal structure of a bacteriophage T7 DNA replication complex at 2.2 Å resolution. *Nature*, **391**, 251–258.
45. Showalter, A. K. & Tsai, M. D. (2002). A reexamination of the nucleotide incorporation fidelity of DNA polymerases. *Biochemistry*, **41**, 10571–10576.
46. Elmendorf, B. J., Shilatifard, A., Yan, Q., Conaway, J. W. & Conaway, R. C. (2001). Transcription factors TFIIF, ELL, and Elongin negatively regulate SII-induced nascent transcript cleavage by non-arrested RNA polymerase II elongation intermediates. *J. Biol. Chem.* **276**, 23109–23114.
47. Gnatt, A. (2002). Elongation by RNA polymerase II: structure-function relationship. *Biochim. Biophys. Acta*, **1577**, 175–190.
48. Shapiro, D. J., Sharp, P. A., Wahli, W. W. & Keller, M. J. (1988). A high-efficiency HeLa cell nuclear transcription extract. *DNA*, **7**, 47–55.
49. Wang, B. Q., Kostrub, C. F., Finkelstein, A. & Burton, Z. F. (1993). Production of human RAP30 and RAP74 in bacterial cells. *Protein Expt. Purif.* **4**, 207–214.
50. Wang, B. Q., Lei, L. & Burton, Z. F. (1994). Importance of codon preference for production of human RAP74 and reconstitution of the RAP30/74 complex. *Protein Expt. Purif.* **5**, 476–485.

Edited by M. Gottesman

(Received 2 May 2004; received in revised form 20 July 2004; accepted 21 July 2004)